Progress in three-terminal heterojunction bipolar transistor solar cells

Elisa Antolín [1,*], Marius H. Zehender [1], Simon A. Svatek [1,2], Myles A. Steiner [3], Mario Martínez[1], Iván García [1], Pablo García-Linares [1], Emily L. Warren [3], Adele. C. Tamboli [3] and Antonio Martí [1]

[1]*Instituto de Energía Solar, Universidad Politécnica de Madrid, Avda. Complutense 30, 28040 Madrid, Spain*
[2] *Departamento de Sistemas Informáticos, Universidad Politécnica de Madrid, C/ Alan Turing s/n, 28031Madrid, Spain*
[3] *National Renewable Energy Laboratory (NREL), 80401 Golden, CO, USA*

** corresponding author: elisa.antolin@upm.es*

Abstract. Conventional solar cells, including multijunction solar cells, are based on *pn* junctions as building blocks. In contrast, the three-terminal heterojunction bipolar transistor solar cell (3T–HBTSC) explores the use of a bipolar transistor structure to build a solar cell. The limiting efficiency of this transistor structure equals that of a double-junction solar cell. However, since the 3T–HBTSC does not require tunnel junctions, its minimal structure has only three semiconductor layers, while the minimal structure of a double junction solar cell has six. This work reviews the operation principles of this solar cell and the steps carried out towards its practical implementation. Experimental results on a GaInP/GaAs HBTSC prototype with bottom interdigitated contacts are presented.

1 Introduction

The three-terminal heterojunction bipolar transistor solar cell (3T-HBTSC) was proposed as the minimal building block to realize a tandem solar cell.[1] Its fundamental structure consists of three semiconductor layers (*npn* or *pnp*) which are called emitter, base and collector, following the convention for bipolar transistors as represented in Fig. 1a. The emitter and base regions are made of wide-bandgap semiconductors and form the *top* junction of the stack. The collector is made of a narrow-bandgap semiconductor. The *bottom* junction is formed by the base and collector regions. Thus, the base region is shared by the *top* and *bottom* subcells. One electric contact is applied to each region, leading to a three-terminal architecture. In contrast, the minimal structure of a conventional two-terminal tandem solar cell based on *pn* junctions, represented in Fig. 1b, requires a minimum of six semiconductor layers, two of them dedicated to the implementation of the tunnel junction.

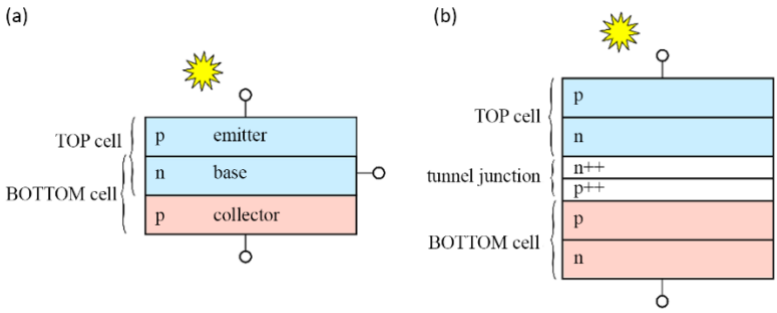

Fig. 1. (a) Minimal structure of a 3T-HBTSC. (b) Minimal structure of a current-matched tandem solar cell.

The term "heterojunction" in the name of the device refers to the fact that at least two different semiconductors are needed in the structure (three if emitter and base are not made of the same material). In principle, any combination of semiconductors can be chosen with bandgap energies appropriate to build an efficient double-junction solar cell.[2] Since it is a three-terminal device, the bandgap energy ranges that can produce high efficiencies are significantly wider than in the case of a current-matched device.[3] The concept is especially useful for emerging technologies in which the fabrication of a tunnel junction can be challenging, such as nanowire devices, or when low-cost epitaxial growth techniques are employed. Practical implementations of the 3T-HBTSC have been proposed based on III-V compounds,[4] earth-abundant kesterites,[5] nanowires,[6,7] and perovskite/silicon.[6,8,9]

What makes the transistor solar cell concept different from other three-terminal architectures [10–12] is the fact that the minority carrier transport through the base is not interrupted, meaning that a majority carrier injected from the emitter into the base (and therefore, becoming a minority carrier in this region) has the potential of reaching the collector, as it is described in the theoretical framework of bipolar transistors.[13] This carrier injection from the emitter and collection by the collector is usually referred to as *transistor effect*. Then, the question arises as whether the transistor effect enhances or worsens the performance of the solar cell with respect to a traditional double-junction device. The answer to this question is given in Section 2 in this paper along with a short review of the theoretical fundamentals of the 3T-HBTSC. The issue of stringing is reviewed in Section 3, and possible base terminal designs in Section 4. In Section 5 we present the characterization of a GaInP/GaAs 3T-HBTSC prototype with interdigitated base/collector contacts at the rear of the cell.

2 Impact of the transistor parameters on the operation of the 3T-HBTSC

Fig. 2 represents the band diagram of a *pnp* 3T-HBTSC solar that we shall use to

illustrate the rationale behind the operation of the 3T-HBTSC. The device is biased at its maximum power point and the dashed lines represent the electron and hole quasi-Fermi (q-F) levels ($E_{F,e}$ and $E_{F,h}$ respectively). The first thing to note in this diagram is that the minority carrier (min-C) q-F level in the base layer, $E_{F,h}$, bends. This is necessary or, otherwise, the output voltage of top and bottom cell (determined by the q-F level split at the base-emitter junction and base-collector junction, respectively) would be the same. In that case, the output voltage of the bottom cell would limit the output voltage of the top cell, and the device would be bound to the efficiency limit of single-gap solar cells.

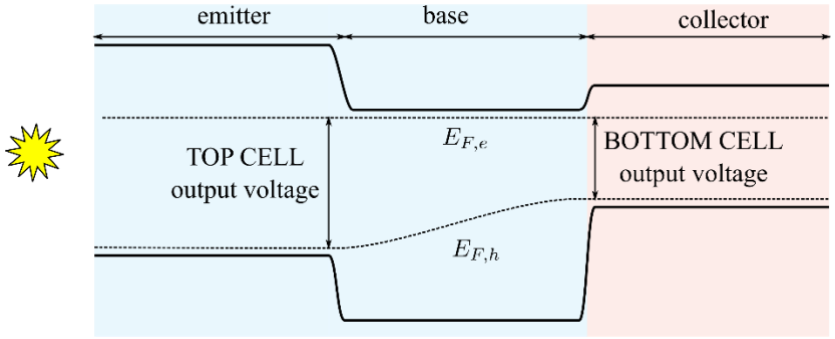

Fig. 2. Simplified band diagram of a *pnp* 3T-HBTSC showing qualitatively the shape of the electron ($E_{F,e}$) and hole ($E_{F,h}$) quasi-Fermi levels for the cell biased at maximum-power point. Finite hole mobility is assumed in the base. For simplicity, carrier mobilities in other regions are assumed to approach infinity. Drawing not to scale.

To understand qualitatively the implications of the q-F level bending, it is useful to recall the generalized current equations for electrons and holes:

$$J_e = \mu_e n \frac{dE_{F,e}}{dx} \quad (1)$$

$$J_h = \mu_h p \frac{dE_{F,h}}{dx} \quad (2)$$

Where $J_{e(h)}$, $\mu_{e(h)}$ and $n(p)$ are respectively the current density, mobility, and carrier density of electrons (holes). These equations apply to any current flow in the device (of minority or majority carriers). They relate said flow to the gradient of the corresponding q-F level. The complete set of equations of the drift-diffusion model of the HBTSC are given in Ref. [14] (in the dark) and Ref. [15] (under illumination). Refs. [8,16] report results obtained with the drift-diffusion model for different HBTSC structures.

According to Eq. (2), to have a non-zero derivative in the base min-C q-F level ($E_{F,h}$) of the 3T-HBTSC the base min-C mobility μ_h must be finite, but this seems to

contradict our notion of ideal solar cell. The two main idealizations applied to calculate the efficiency limit of conventional *pn* junction solar cells are the absence of non-radiative recombination and infinite carrier mobility. [17] The second condition rules out the appearance of ohmic losses and implies that there cannot be gradients in the q-F levels. Contrarily, in a solar cell with transistor structure a min-C q-F level gradient is necessary to reach maximum efficiency. Therefore, we need to eliminate the ohmic losses associated with min-C transport across the base with a different condition. Once infinite min-C mobility has been ruled out, the remaining option is to suppress the min-C current density itself across the base.

The min-C current density in the base can be minimized by preventing electron-hole pair generation and recombination in that region, which, in the radiative limit, can be approached by increasing its bandgap energy. With respect to the photogeneration, when the gap increases, the energy of most solar photons is not large enough to excite an electron from the valence band to the conduction band, and carrier generation is inhibited. Not exploiting photon absorption in the base has no impact on the ideal device because it can be assumed that the emitter and the collector absorb all photons with energy above their bandgaps. And with respect to thermal generation/recombination, the rate of those processes also decreases if the bandgap energy increases. This argument can also be understood by considering that the min-C concentration approaches zero as the bandgap energy increases and, as it can be seen in Eqs. (1) and (2), this produces the desired effect of making the min-C current density approach zero.

It is also possible to reduce the min-C concentration in the base region by increasing the dopant concentration as long as high doping effects do not become detrimental to the device performance. A high base doping level can, on the other hand, facilitate the implementation of the metal-semiconductor contact on the base and prevent ohmic losses associated to the lateral extraction of majority carriers in that region.[4]

Within the theoretical framework of bipolar transistors, the suppression of the min-C carrier concentration and min-C current density in the base prevents the injection of carriers from the adjacent layers, resulting in emitter and collector carrier injection efficiencies close to zero. On the other hand, we have seen that choosing a wide bandgap semiconductor for the base is associated to a low thermal generation/recombination rate and, if non-radiative processes are inhibited, we can expect a large min-C diffusion length in the base, that is, a base in which the transport factor approaches one. Therefore, we conclude that the conditions that maximize the conversion efficiency in transistor solar cells are associated to *low injection efficiencies* and *high transport factors*. Note that in the case of a transistor, a low injection efficiency, even in the presence of a high transport factor, would prevent the transistor effect, that is, would result in a bad transistor, one without amplification properties.[18]

The arguments above are useful to understand the optimum configuration of ideal 3T-HBTSCs, but in practical cells it is necessary to find compromises. For example,

pursuing a base with an extremely wide bandgap could require low quality materials or materials that cannot be effectively *n* doped, for a *pnp* 3T-HBTSC, or effectively *p* doped, in the case of an *npn* structure. Also, if the emitter of the cell does not work in the radiative limit, it might be advisable to reduce its thickness and implement a base region with a moderate bandgap, so that the base absorbs a portion of the light providing better collection efficiency than a non-optimal emitter. It has been demonstrated that in realistic 3T-HBTSC designs a base with a moderately high doping and moderately large bandgap energy – suitable to contribute to photon absorption - can have a negligible minority carrier concentration and prevent the appearance of the transistor effect.[14]

3 The issue of module stringing

The use of a three-terminal solar cell poses the problem of how to interconnect the terminals of several devices to achieve a module output voltage that is sufficient for practical applications.[19,20] In this respect, Gee[21] provided a partial solution that sacrifices two solar cells in the array and demands the output voltage of the top cell to be an integer multiple of the output voltage of the bottom cell. This approach was experimentally verified using AlGaAs/GaAs 3T-HBTSCs by Zehender *et al.*[22] The voltage-matching configuration of three-terminal devices has been extensively studied by McMahon *et al.*[23]

An attractive solution to the stringing problem is to stack a 3T-HBTSC on top of a silicon cell,[24] as illustrated in Fig. 3, interconnecting the two sub-cells by a conductive transparent adhesive such as the one described by Klein *et al.*[25] Connecting the top contact (T) of the 3T-HBTSC to the rear contact of the Si cell leads to a two-terminal triple-junction solar cell using voltage matching. Remarkably, if the 3T-HBTSC is made of GaInP/GaAs, the resulting triple-junction device has a limiting efficiency of 43% (AM1.5 G spectrum).[24] Also, the efficiency is tolerant against spectral changes thanks to the combination of a parallel interconnection and a series interconnection (see the circuit diagram on the left side of Fig. 3). Using GaInP/GaAs and silicon poses the advantage of combining two mature solar cell technologies.

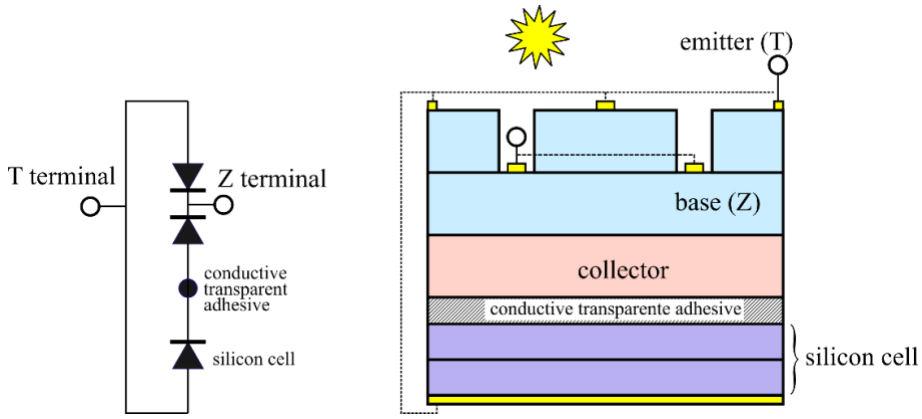

Fig. 3. Schematic representation of a GaInP/GaAs 3T-HBTSC on top of a silicon cell to produce a 2-terminal triple-junction solar cell. The equivalent circuit shown at the left illustrates the contacting scheme between the cells.

4 Design of electric contacts

Following the general taxonomy for three-terminal solar cells proposed by Warren *et al.* [26] the three terminals on a 3T-HBTSC are denoted: T (emitter), Z (base), and R (collector). An important practical question in the implementation of this device is the design of the Z terminal. At this respect, two approaches have been considered. In the first one (Fig. 4a) the base is accessed from the top with a top interdigitated contact (TIC). In the second approach, the base is accessed from the bottom (Fig. 4b) using a bottom interdigitated contact (BIC). In principle, the BIC approach is expected to enable a higher efficiency because of its lower shadowing factor, since in this design the base metal fingers can be aligned underneath the emitter metal fingers. However, the fabrication of a BIC 3T-HBTSC can be difficult in some cases, for instance when the device is intended to be part of a triple-junction stack as the one shown in Fig. 3. With either TIC or BIC configuration, having a high doping level in the base – besides eliminating the transistor effect – reduces ohmic losses associated to the lateral flow of carriers in the base and facilitates the implementation of the base terminal. Practical details for the implementation of the base metal contact have been reported by Martínez *et al.*[27]

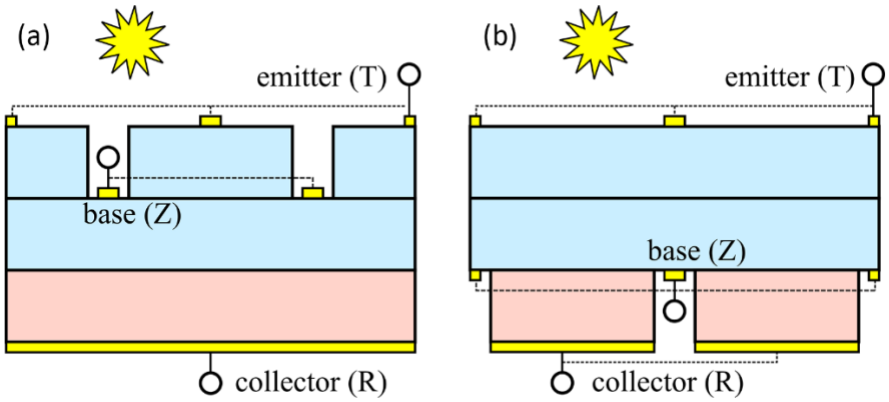

Fig. 4. Illustration of interdigitated contact scheme in which the base is contacted (a) from the top (TIC scheme) and (b) from the bottom (BIC scheme).

5 Characterization of a BIC 3T-HBTSC prototype

3T-HBTSC devices of both types, applying either the TIC or BIC scheme, have been manufactured in collaboration between the National Renewable Energy Laboratory (USA) and the Instituto de Energía Solar - Universidad Politécnica de Madrid (Spain). The semiconductor structures are grown epitaxially by metal-organic chemical vapor deposition (MOCVD). They consist of a GaInP emitter, (Al)GaInP base and GaAs collector, along with typical passivation and contacting layers for emitter and collector. Following the three-terminal device taxonomy[26] the structures are denoted GaInP/r/GaAs(p/n). Device fabrication is performed using wet or dry etching, photolithography, and thermal evaporation combined with rapid thermal annealing to produce the metallizations.

As a result of this work, an experimental proof-of-concept for the 3T-HBTSC has been reported. [4] The experiments were performed on a TIC GaInP/GaInP/GaAs *npn* prototype, and it was possible to demonstrate a large voltage difference between the two junctions and independent power extraction (no crosstalk between junctions for irradiances lower than or equal to one sun). The contribution of the base region to the photocurrent of either junction was also shown. The device included an optimized anti-reflection coating (ARC). The total efficiency of the proof-of-concept 3T-HBTSC under AM1.5G spectrum was (27.8 ± 2.9) % considering the illuminated area (neglecting the area covered by metal or etched to expose the base layer) and (18.2 ± 1.6) % considering the mesa area (the total device area, including shadowed parts).

Here we present the results of a BIC 3T-HBTSC prototype. The semiconductor structure was grown epitaxially on a GaAs substrate in an inverted order, with the front of the device grown first and the back contact layer grown last. This facilitated the fabrication of the base and collector metal contacts on the top of the wafer. Then

the structure was turned over and glued to a silicon handle, and the substrate was chemically removed. Finally, the emitter metal fingers were deposited, aligning them on top of the base metal fingers. Further details on the step-by-step fabrication procedure have been given in Ref.[28] and the modeling and design of the BIC metal grid will be reported elsewhere.[29] The parameters of the semiconductor layer structure are compiled in Table 1. Fig. 5a shows a photograph of a completed device and Fig. 5b shows a photograph of a device as it shines due to electroluminescence in the GaInP layers under current injection in the top junction. The devices have no ARC and the mesa area is 4.04 mm^2.

Table 1: Layer structure of the BIC 3T-HBTSC prototype (sample MT220). The layers are ordered as in the final orientation of the device (the epitaxial structure was grown inverted). Layer thicknesses have been determined in-situ from the oscillations in the reflected power of a laser beam impinging the growth surface - k-Space multibeam optical stress (MOS) sensor - or ex-situ from profiler measurements on etched samples, except for the values of the two first layers, which are nominal. Dopant concentrations have been extracted from secondary ion mass spectroscopy (SIMS) measurements.

Layer	Thickness (nm)	Material	Dopant concentration (cm^{-3})
T-terminal contact	300	GaInAsN:Se GaAs:Se	$4{\cdot}10^{19}$
Window	20	AlInP:Se	$9{\cdot}10^{18}$
Emitter	328	GaInP:Si	$7{\cdot}10^{17}$
Base	964	GaInP:Zn	$5{\cdot}10^{18}$
Collector	1312	GaAs:Si	$7{\cdot}10^{17}$
Back surface field (BSF)	159	GaInP:Si	$7{\cdot}10^{17}$
R-terminal contact	113	GaAs:Se,Si	$7{\cdot}10^{18}$

Fig. 5c shows the external quantum efficiency (EQE) of the BIC 3T-HBTSC prototype, which is characteristic of a double-junction GaInP/GaAs device without ARC. Fig. 5d presents the current density (J) -voltage (V) curves measured under illumination with the AM1.5G spectrum. The parameters extracted from those curves are compiled in Table 2. It is remarkable that the J-V curves measured for each junction when the other junction was in open circuit (OC), maximum power point (MPP) or short circuit (SC) are virtually identical, except for an increase in the photocurrent of the bottom junction when the top junction is at OC. The origin of this extra photocurrent could be a residual transistor effect, which would be noticeable when the top junction is at OC but not when it is at MPP, in agreement

with the results of the theoretical modelling of HBTSC structures.[16] It is also plausible that the excess photocurrent is caused by luminescent coupling, which is commonly observed in high-quality epitaxial GaInP/GaAs mutijunction solar cells.[30] In future works, the multiple fitting of dark *J-V* curves - measured with different voltage biases at the not-measured junction – could probably be used to discriminate between the two mechanisms.

The absence of crosstalk between subcells is further observed in the *V-V* maps presented in Fig. 6 (a general discussion on *V-V* plots that characterize three-terminal devices can be found in Ref. [26]). Here it can be seen that the photocurrent density and output power of the top junction only depends on its own bias (Fig. 6a and c). The same applies to the bottom junction (Fig. 6b and d), except for the effect of luminescent coupling and/or transistor effect that is observed in the right extreme of the bottom junction plots. The fact that the power extraction from either junction is independent of the working point for voltages lower or equal to the MPP voltage of the other junction demonstrates the absence of a transistor effect in this device under operation conditions.

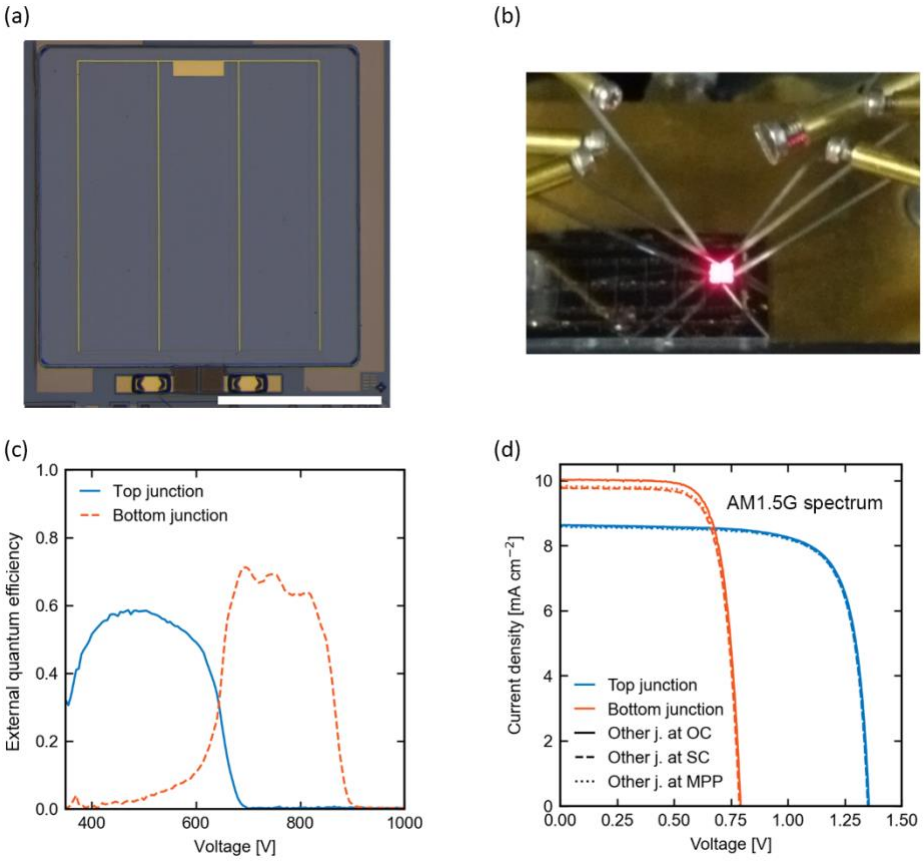

Fig. 5. (a) Top view of a BIC 3T-HBTSC device (sample MT220). Scale bar is 1 mm. (b) Photograph of the device under current injection, showing electroluminescence from the

GaInP layers. (c) EQE of the BIC 3T-HBTSC device. (d) Current-voltage characteristics of the top and bottom junctions measured when the other junction is at open-circuit (solid lines), maximum power point (dotted lines), and short-circuit (dashed lines).

The AM1.5G efficiency of the BIC 3T-HBTSC prototype is 14.6% (with no ARC) of which 8.8% originates in the top junction and 5.8% in the bottom junction. It is important to note that we have used the same area to scale the efficiencies of both junctions: the mesa area, which contains the whole device (4.04 mm^2). Therefore, the impact of extra shadowing in the bottom junction - due to the regions that have been etched to implement the Z contact - is accounted for in the resulting efficiency. The bottom junction shadowing factor is 8% (in this device the grooves that allocate the base metal fingers are 30 μm wide, and the grid fingers are 10 μm wide; using industrial photolithography equipment the width of the grooves could be significantly reduced). The fill factors (FF) and open-circuit voltages (V_{OC}) in this BIC 3T-HBTSC are lower than the ones reported for the TIC device in Ref. [4]. Possible factors that can contribute to this discrepancy are: (i) a larger dark current component arising from perimeter recombination in the collector etch walls in the case of the BIC proof-of-concept device (GaAs is known to suffer from stronger perimeter recombination than GaInP) [31], (ii) a non-optimal implementation of the Z contact in this structure (the BIC device has a simple Au/Zn/Au metallic contact whereas the TIC device has a compensated contact [27]), and/or (iii) the processing complexity introduced by the use of an inverted structure.

Table 2: Parameters of the BIC 3T-HBTSC prototype under illumination with the AM1.5G spectrum. The area considered to calculate photocurrent densities and efficiencies is the mesa area.

Top junction	
J_{SC} (mA/cm^2)	8.6
V_{OC} (V)	1.35
FF (%)	76
η (%)	8.8
Bottom junction	
J_{SC} (mA/cm^2)	9.8
V_{OC} (V)	0.79
FF (%)	74
η (%)	5.8

Cumulative:	
η (%)	14.6

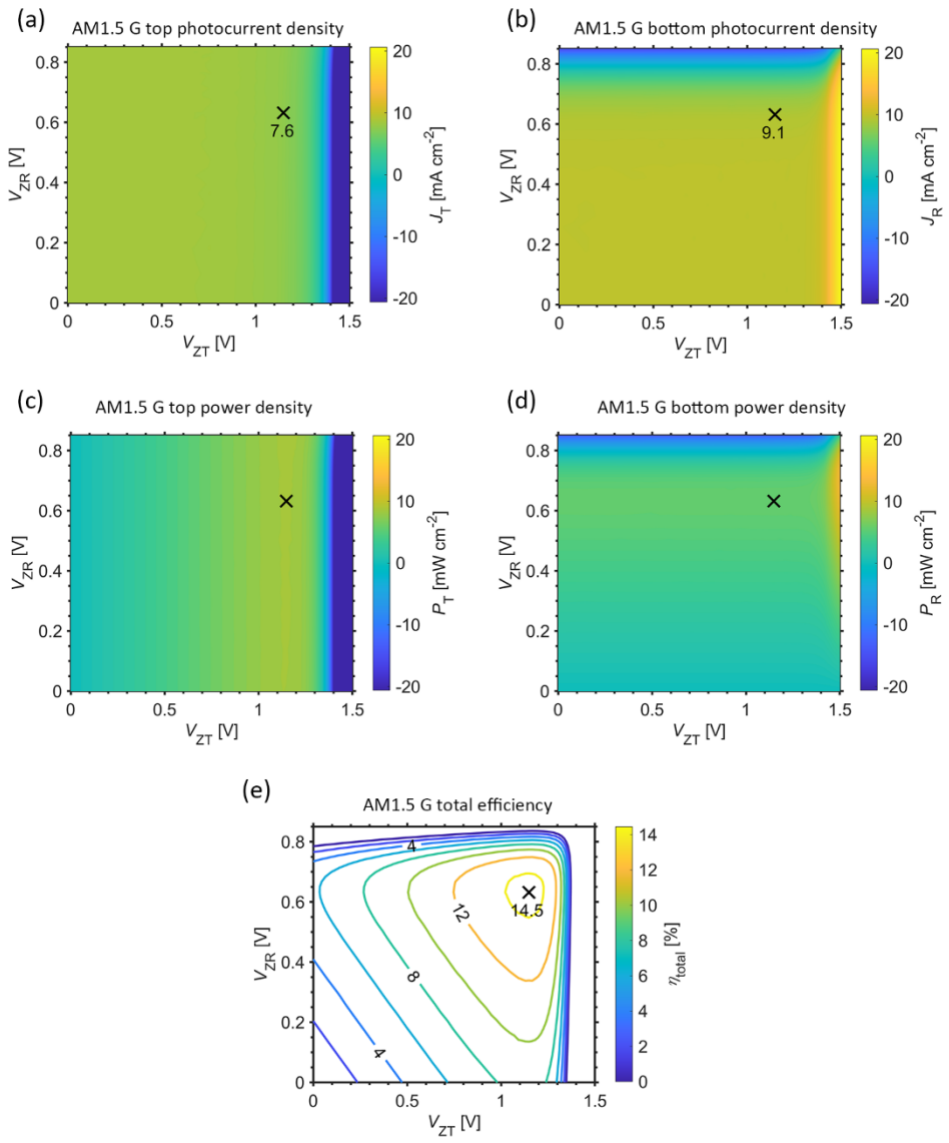

Fig. 6. Measurement of different parameters on the BIC HBTSC prototype under illumination with the AM1.5G spectrum as a function of the voltage bias at the top junction (V_{ZT}) and voltage bias at the bottom junction (V_{ZR}). (a) Photocurrent measured on the top junction. (b) Photocurrent measured on the bottom junction. (c) Power density measured on the top junction. (d) Power density measured on the bottom junction. (d) Total efficiency resulting from the sum of the power on both subcells.

6 Conclusions

In this paper the operation principles of the 3T-HBTSC are reviewed, with emphasis on the importance of preventing the transistor effect to achieve a high efficiency. A possible combination of a 3T-HBTSC with a silicon bottom cell to form a two-terminal triple-junction solar cell has been discussed as a strategy to increase the conversion efficiency and circumvent the stringing problem. Two possible device designs have been proposed for the 3T-HBTSC in which the base contact is either interdigitated with the emitter contact on the top surface or interdigitated with the collector contact on the rear surface. Finally, experimental results of a GaInP/GaAs 3T-HBTSC prototype with a bottom interdigitated contacts have been presented which show independent power extraction from the top and bottom junctions under operation conditions.

Acknowledgments

The authors would like to thank Irene Artacho and Miguel Gómez from IES-UPM for technical support and Waldo Olavarria from NREL for help with MOCVD growth. This work has been partially supported by the grant RTI2018-096937-B-C21 (MULTIPLIER) funded by MCIN/AEI/ 10.13039/501100011033 and "ERDF A way of making Europe", and by grant 787289 (GRECO) funded by the European Union's Horizon2020 Research and Innovation Programme. E.A. acknowledges grant RYC-2015-18539 (Ramón y Cajal Fellowship) and M.M. acknowledges grant PRE2019-087894 (Formación del Personal Investigador Predoctoral Fellowship), both funded by MCIN/AEI/ 10.13039/501100011033 and by "ESF Investing in your future". M.H.Z. is grateful to Universidad Politécnica de Madrid for funding from 'Programa Propio para Ayudas Predoctorales de la UPM'. Partial funding provided by the U.S. Department of Energy, Office of Energy Efficiency and Renewable Energy, Solar Energy Technology Office under contracts DE-00034911 and DE-00034358. The views expressed in the article do not necessarily represent the views of the DOE or the U.S. Government. The U.S. Government retains and the publisher, by accepting the article for publication, acknowledges that the U.S. Government retains a nonexclusive, paid-up, irrevocable, worldwide license to publish or reproduce the published form of this work, or allow others to do so, for U.S. Government purposes.

References

1. Martí A, Luque A. Three-terminal heterojunction bipolar transistor solar cell for high-efficiency photovoltaic conversion. *Nat Commun*. 2015;6(1):6902. doi:10.1038/ncomms7902

2. Martí A, Araújo GL. Limiting efficiencies for photovoltaic energy conversion in multigap systems. *Sol Energy Mater Sol Cells*. 1996;43:203-222. doi:10.1016/0927-0248(96)00015-3

3. Yu Z (Jason), Leilaeioun M, Holman Z. Selecting tandem partners for silicon solar cells. *Nat Energy*. 2016;1:16137. doi:10.1038/nenergy.2016.137

4. Zehender MH, Svatek SA, Steiner MA, et al. GaInP/GaAs three-terminal heterojunction bipolar transistor solar cell. Under review in Nat. Commun. The preprint can be found in: doi:10.21203/rs.3.rs-113488/v1

5. Saha U, Alam MdK. A heterojunction bipolar transistor architecture-based solar cell using CBTSSe/CdS/ACZTSe materials. *Sol Energy*. 2019;184:664-671. doi:10.1016/j.solener.2019.04.044

6. Linares PG, Antolín E, Martí A. Novel heterojunction bipolar transistor architectures for the practical implementation of high-efficiency three-terminal solar cells. *Sol Energy Mater Sol Cells*. 2019;194:54-61. doi:10.1016/j.solmat.2019.01.027

7. Zehender MH, Chen Y, Barrigón E, Martí A, Borgström MT, Antolín E. Design study of a nanowire three-terminal heterojunction bipolar transistor solar cell. In: *48th IEEE PVSC. Published Online 2021*.

8. Giliberti G, Martí A, Cappelluti F. Perovskite-Si solar cell: a three-terminal heterojunction bipolar transistor architecture. In: *2020 47th IEEE Photovoltaic Specialists Conference (PVSC)*. ; 2020:2696-2699. doi:10.1109/PVSC45281.2020.9300949

9. Wahid S, Alam MdK. Efficiency Enhancement of Perovskite Solar Cells Using Heterojunction Bipolar Transistor Configuration. *IEEE Trans Electron Devices*. 2020;67(2):552-557. doi:10.1109/TED.2019.2961005

10. Flores C. A three-terminal double junction GaAs/GaAlAs cascade solar cell. *IEEE Electron Device Lett*. 1983;4:96-99. doi:10.1109/EDL.1983.25662

11. Steiner MA, Wanlass MW, Carapella JJ, et al. A monolithic three-terminal GaInAsP/GaInAs tandem solar cell. *Prog Photovolt Res Appl*. 2009;17(8):587-593. doi:10.1002/pip.913

12. Wanlass MW, Coutts TJ, Ward JS, Emery KA, Gessert TA, Osterwald CR. Advanced high-efficiency concentrator tandem solar cells. In: *The Conference Record of the Twenty-Second IEEE Photovoltaic Specialists Conference - 1991*. ; 1991:38-45 vol.1. doi:10.1109/PVSC.1991.169179

13. Shockley W. The theory of p-n junctions in semiconductors and p-n junction transistors. *Bell Syst Tech J*. 1949;28(3):435-489. doi:10.1002/j.1538-7305.1949.tb03645.x

14. Antolin E, Zehender MH, Garcia-Linares P, Svatek SA, Marti A. Considerations for the Design of a Heterojunction Bipolar Transistor Solar Cell. *IEEE J Photovolt*. 2019;10(1):2-7. doi:10.1109/JPHOTOV.2019.2945914

15. Martí A, Antolín E, Zehender MH, et al. Cuaderno abierto para la simulación de células solares de tres terminales de tipo transistor bipolar de heterounión. *CIES2020 - XVII Congr Ibérico E XIII Congr Iberoam Energ Sol*. Published online November 2020:23-31. doi:10.34637/cies2020.1.1001

16. Giliberti G, Bonani F, Martí A, Cappelluti F. Modeling of three-terminal heterojunction bipolar transistor solar cells. In: *2020 International Conference on Numerical Simulation of Optoelectronic Devices (NUSOD)*. ; 2020:43-44. doi:10.1109/NUSOD49422.2020.9217745

17. Araújo GL, Martí A. Absolute limiting efficiencies for photovoltaic energy conversion. *Sol Energy Mater Sol Cells*. 1994;33(2):213-240. doi:10.1016/0927-0248(94)90209-7

18. Ebers JJ, Moll JL. Large-Signal Behavior of Junction Transistors. *Proc IRE*. 1954;42(12):1761-1772. doi:10.1109/JRPROC.1954.274797

19. Schulte-Huxel H, Friedman DJ, Tamboli AC. String-Level Modeling of Two, Three, and Four Terminal Si-Based Tandem Modules. *IEEE J Photovolt*. 2018;8(5):1370-1375. doi:10.1109/JPHOTOV.2018.2855104

20. Geisz JF, McMahon WE, Buencuerpo J, Rienäcker M, Tamboli AC, Warren EL. Unique Characterization of Three-Terminal Photovoltaic Devices. *Rev Joule*. Published online 2021.

21. Gee JM. A comparison of different module configurations for multi-band-gap solar cells. *Sol Cells*. 1988;24(1):147-155. doi:10.1016/0379-6787(88)90044-0

22. Zehender M, Antolín E, García-Linares P, et al. Module interconnection for the three-terminal heterojunction bipolar transistor solar cell. *AIP Conf Proc*. 2018;2012(1):040013. doi:10.1063/1.5053521

23. McMahon WE, Schulte-Huxel H, Buencuerpo J, et al. Homogenous Voltage-Matched Strings Using Three-Terminal Tandem Solar Cells: Fundamentals and End Losses. *IEEE J Photovolt*. 2021;11(4):1078-1086. doi:10.1109/JPHOTOV.2021.3068325

24. Antolin E, Zehender MH, Svatek SA, Garcia-Linares P, Marti A. III-V-on-silicon triple-junction based on the heterojunction bipolar transistor solar cell concept. In: *47th IEEE Photovoltaics Specialist Conference (PVSC)*. ; 2020:1226-1231. doi:10.1109/pvsc45281.2020.9300681

25. Klein TR, Lee BG, Schnabel M, et al. Transparent Conductive Adhesives for Tandem Solar Cells Using Polymer-Particle Composites. *ACS Appl Mater Interfaces*. 2018;10(9):8086-8091. doi:10.1021/acsami.8b00175

26. Warren EL, McMahon WE, Rienäcker M, et al. A Taxonomy for Three-Terminal Tandem Solar Cells. *ACS Energy Lett*. 2020;5(4):1233-1242.

doi:10.1021/acsenergylett.0c00068

27. Martínez M, Svatek SA, Zehender MH, et al. Compensated contacts for three-terminal transistor solar cells. *48th IEEE PVSC*. Published online 2021.

28. Zehender MH, Svatek SA, Steiner MA, et al. Inverted GaInP/GaAs Three-Terminal Heterojunction Bipolar Transistor Solar Cell. In: *47th IEEE Photovoltaic Specialists Conference (PVSC)*. ; 2020:1517-1521. doi:10.1109/PVSC45281.2020.9301000.

29. Zehender MH, et al. Series resistance in three-terminal heterojunction bipolar transistor solar cells. Published online 2021.

30. Steiner MA, Geisz JF. Non-linear luminescent coupling in series-connected multijunction solar cells. *Appl Phys Lett*. 2012;100(25):251106. doi:10.1063/1.4729827

31. Aspnes DE. Recombination at semiconductor surfaces and interfaces. *Surf Sci*. 1983;132(1):406-421. doi:10.1016/0039-6028(83)90550-2